

Training and Tuning Generative Neural Radiance Fields for Attribute-Conditional 3D-Aware Face Generation

Jichao Zhang, Aliaksandr Siarohin, Yahui Liu, Hao Tang, Nicu Sebe, *Senior Member, IEEE*, and Wei Wang

Abstract—Generative Neural Radiance Fields (GNeRF) based 3D-aware GANs have demonstrated remarkable capabilities in generating high-quality images while maintaining strong 3D consistency. Notably, significant advancements have been made in the domain of face generation. However, most existing models prioritize view consistency over disentanglement, resulting in limited semantic/attribute control during generation. To address this limitation, we propose a conditional GNeRF model incorporating specific attribute labels as input to enhance the controllability and disentanglement abilities of 3D-aware generative models. Our approach builds upon a pre-trained 3D-aware face model, and we introduce a Training as Init and Optimizing for Tuning (TRIOT) method to train a conditional normalized flow module to enable the facial attribute editing, then optimize the latent vector to improve attribute-editing precision further. Our extensive experiments demonstrate that our model produces high-quality edits with superior view consistency while preserving non-target regions. Code is available at <https://github.com/zhangqianhui/TT-GNeRF>.

Index Terms—Generative Neural Radiance Fields, Face Image Generation and Editing



1 INTRODUCTION

High-quality image generation and semantic disentanglement are longstanding goals in computer vision and computer graphics. In the past few years, Generative Adversarial Networks (GANs) [1] and their variants have garnered significant attention for their ability to produce high-quality image generation and editing. These methods have greatly improved visual fidelity, rendering speed, and interactive controls compared to traditional computer graphics pipelines.

Numerous prior works [2], [3], [4], [5] have focused on realistic face editing. These approaches either rely on image-to-image translation models [2], [6] or leverage the disentanglement abilities [3], [4], [5] of StyleGAN [7], [8]. These methods can be broadly classified into supervised and unsupervised categories. Unsupervised methods typically search for interpretable directions using PCA [9] or introduce soft orthogonality constraints [10], [11] in the latent space. However, these approaches provide only coarse controls. Supervised methods [2], [3], on the other hand, utilize specific attribute labels as conditions. However, these methods lack precise control over 3D factors such as camera pose because

they overlook the underlying 3D scene rendering process. To address this issue, some works [4], [12] have integrated 3D Morphable Face Models (3DMM) [13] to enable control over 3D face pose and facial expression. Nonetheless, these approaches still suffer from significant challenges, such as view inconsistency and unrealistic texture distortion when poses are drastically varied.

Recently, neural radiance fields (NeRF) [14] have attracted booming attention because of their impressive results in novel view-rendering tasks. Specifically, NeRF represents a scene using a continuous function parameterized by a multi-layer perceptron (MLP) that maps a 3D position and a viewing direction to density and radiance values. Since then, many works have been proposed to improve NeRF [15], [16] and apply it to various downstream tasks, such as human body modeling [17] and large scene modeling [18].

Some 3D-aware image generation methods [19], [20] combine NeRF with generative models by extending neural radiance fields with latent conditioning, called Generative Neural Radiance Fields (GNeRF). 3D coordinates are sampled from random camera poses and used as input to an implicit function with latent codes. This function predicts density and RGB color. However, these methods are compute-intensive and memory inefficient due to sampling many rays in the entire 3D-volume space and requiring a feed-forward process for each point. They are limited to low-resolution and low-quality generation. GIRAFFE [21] addresses this by generating low-resolution feature fields and using a convolution-based neural rendering module to map rendered features into high-resolution output. However, it suffers from serious view-inconsistency problems. To improve generation quality and view-consistency, many approaches [22], [23], [24] borrow ideas from StyleGAN

- Jichao Zhang, Nicu Sebe are with the Department of Information Engineering and Computer Science (DISI), University of Trento, Italy. E-mail: jichao.zhang@unitn.it.
- Aliaksandr Siarohin is with the Snap Research, Santa Monica, CA, US. E-mail: aliaksandr.siarohin@gmail.com.
- Yahui Liu is a Principal Engineer in Huawei, Shenzhen, China. E-mail: yahui.cvr@gmail.com.
- Hao Tang is with the Department of Information Technology and Electrical Engineering, ETH Zurich, Switzerland. E-mail: hao.tang@vision.ee.ethz.ch.
- Wei Wang is with the Institute of Information Science, Beijing Jiaotong University, Beijing, China. E-mail: wangwei1990@gmail.com.

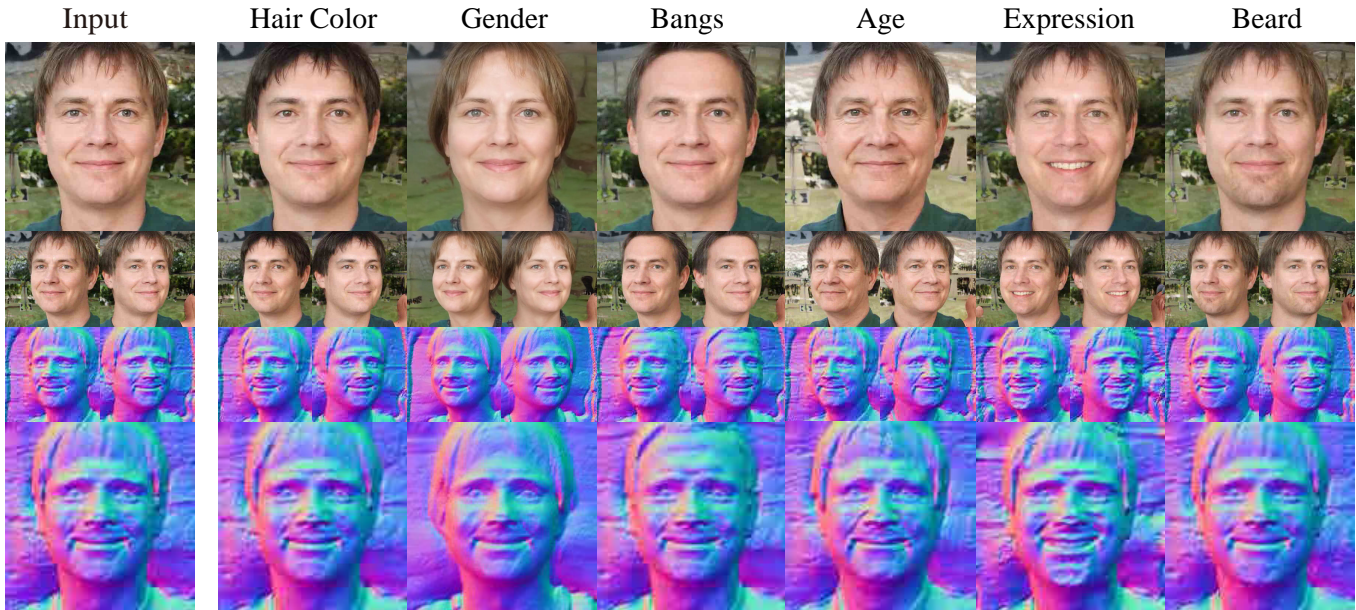


Fig. 1. Our method produces controllable 3D-aware face generation (first two rows) given specific attributes as guidance and the corresponding normals (bottom two rows). As shown in the normal images, the geometry has been preserved for the attribute “Hair Color”, while the mouth region of the “Smiling” mesh has changed.

and integrate the ‘Style-modules’ into the implicit function (e.g., SIREN [20]) or neural rendering module. Some novel algorithms and losses have been carefully designed for 3D-aware generation, such as tri-planes [23] or multiple-view warping loss [24]. While these models create high-quality, view-consistent images, they lack control and disentangling abilities. As explained in VolumeGAN [25], some models are limited to local receptive fields with MLPs, and it is hard to extract global structures from their internal representation. Thus, VolumeGAN utilizes a 3D feature volume module for querying coordinate descriptors, enabling independent controls on the texture and structure factors. However, VolumeGAN still faces challenges regarding quality and view consistency and does not support attribute controls for face manipulation.

We have developed an attribute-conditional 3D-aware generative model to control facial attributes and address the aforementioned issues. Recently, some papers [26], [27], [28] utilize the semantics or 3DMM prior as the condition to edit and control the 3D face avatar. Our model differs from them in two significant ways. Firstly, our model utilizes attribute labels as the condition to achieve different tasks (facial multiple attribute editing). Secondly, we use a pre-trained 3D-aware GNeRF as the backbone of our model, eliminating the need for retraining. We have proposed the “Training-As-Init, Optimizing-for-Tuning” method (TRIOT) to achieve latent disentanglement for accurate facial attribute editing. Our TRIOT consists of two steps. First, we follow the previous 2D method [3] to train the conditional normalizing flow to learn the distribution of latent space, enabling multiple attribute editing by giving the labels. Second, we use the edited latent vector for target attributes as initialization to improve the editing accuracy and better preserve the non-target regions in images. We then optimize this latent vector with the proposed semantic-guided texture and geometry consistency losses while fixing the rest of the

model. Finally, we present an unsupervised optimization method for reference-based facial geometry transfer (See the Fig. 4).

In summary, the main contributions of this work are:

- 1) We propose a “Training-as-Init, Optimizing-for-Tuning” (TRIOT) method, combining the module-training and latent-optimization method for disentangling latent space and enabling attribute-editing tasks.
- 2) Our method is flexible, and general and can be easily integrated into most 3D-Aware GAN backbones.
- 3) Compared to baseline models, our model achieves high-quality editing with improved view consistency while preserving non-target regions.
- 4) We propose an unsupervised optimization method for reference-based geometry transfer task.

2 RELATED WORK

Generative Neural Radiance Fields for 3D-Aware Face Generation. Neural radiance fields (NeRF) [14], a continuous neural mapping from a 3D position and a 2D viewing direction to the RGB value and density that allows 3D scene modeling and high-quality novel view synthesis. Recently, several NeRF-based methods were proposed to improve rendering speed [16], [29], [30] and rendering quality [31], [32], [33]. Moreover, NeRF also promotes the development of many computer-graphics applications, such as human body modeling [17], [34], 3D-aware face generation [21], [22], [23], [25], [35], [36], [37], large scene modeling [18], and pose estimation [19].

Generative neural radiance fields (GNeRF) are a conditional variant of NeRF, which combines NeRF with GANs to condition the rendering process on a latent code that governs the object’s appearance and shape [19], [20], [21]. For example, GRAF [38] achieves this goal by incorporating

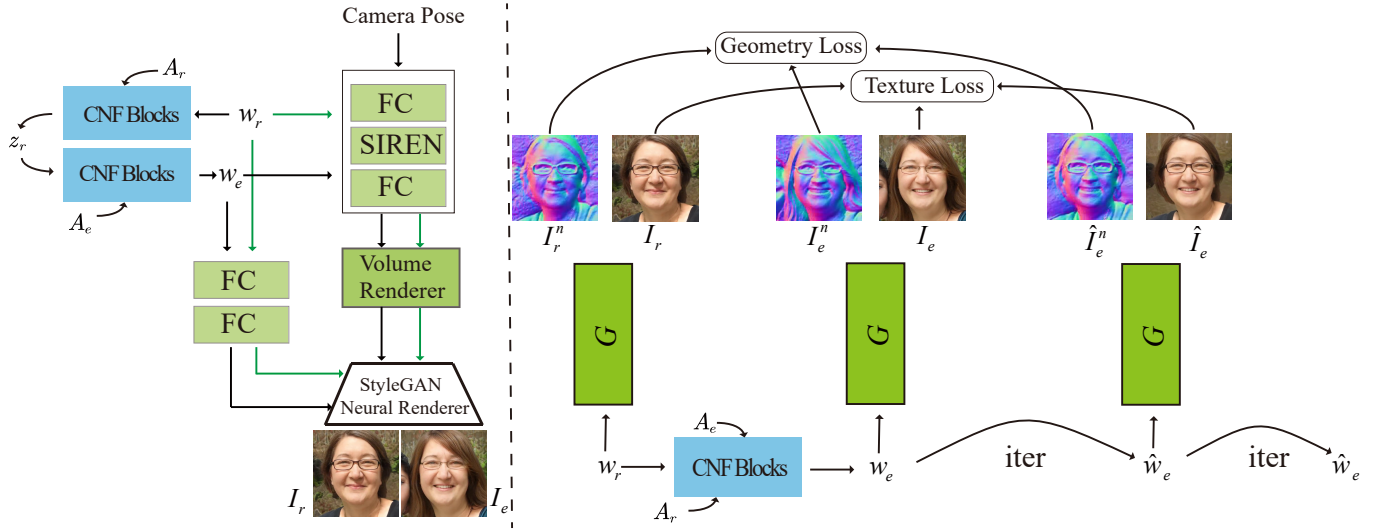


Fig. 2. “Training as Init, Optimizing for Tuning” method overview (Attribute “Expression” as an example). First, given the pretrained StyleSDF [22], we follow StyleFlow to train the continuous normalized flows (CNF) to learn the conditional distribution of latent code w (Left). The attribute editing can be enabled by given target labels A_e to manipulate the latent code. Second, we regard the edited latent code w_e as the initial result, then iteratively optimize the latent code w_e to search for a better one by using proposed geometry and texture consistency objective functions (Right).

shape and appearance codes as input. GRAF [38] achieves better visual fidelity and view consistency than the previous voxel- and feature-based methods [39], [40]. Michael *et al.* [21] propose the compositional neural feature fields (GIRAFFE) that extend GRAF into 3D-aware multiple-object scene representations. Although GRAF and GIRAFFE can control texture and camera pose, they are limited to low-resolution results and fail to preserve multi-view consistency. Many works [20], [22], [23], [24], [35], [41], [42], [43], [44], [45], [46], [47] are trying to address these problems, and most of them inherit the “image-as-style” idea from StyleGAN [8]. Yang *et al.* [44] extend the GIRAFFE to work with high-resolution data. However, this model still suffers from the view-inconsistency problems. Pi-GAN [20] proposes a SIREN module with periodic activation functions. It conditions the style code by feature-wise linear modulation (FILM). The SIREN modules significantly boost image quality and view consistency. To reduce the high computational costs of the volume rendering in Pi-GAN, some models, such as StyleSDF [22], MVCGAN [24] and EG3D [23] propose a hybrid rendering approach. Specifically, they learn a coarse feature field, render it into a low-resolution feature map, and then utilize a style-based 2D network as a “super-resolution” module to refine the features for a final high-resolution image. In order to improve view consistency, StyleSDF models signed distance fields, while MVCGAN uses explicit multi-view consistency loss. On the other hand, ED3D proposes a hybrid 3D tri-plane representation. Unlike the mentioned works, CIPS-3D [41] keeps the resolution of intermediate feature fields the same as the resolution of the final images. These models can achieve incredible quality generation with strong view consistency, but they cannot edit structures and textures.

Recently, some research has focused on the disentangling abilities of 3D-aware models. VolumeGAN [25] tries to separate shape from texture, while ShadeGAN [43] disentangles the light from the albedo. However, they only focus on global factors, such as illumination and textures,

and cannot handle more specific attributes, such as hair color and gender. Some of the concurrent methods [27], [28] provide high-quality expression control but are limited in handling diverse attributes, requiring the model to be trained from scratch. In similar work, LENErf [48] utilizes the CLIP losses to train 3D GAN for text-guided facial attribute editing tasks. Compared to this method, which focuses on local attributes, we utilize the attribute binary labels to guide the editing for global and local attributes.

Image-to-Image Translation Architectures for Face Editing. Image-to-Image translation models, *i.e.*, Pix2Pix [49] and CycleGAN [50], utilize the autoencoder as a generator that has been widely adopted for a variety of different tasks, including face attribute editing [2], [6], [51], [52], [53], [54], [55], [56], [57]. Specifically, StarGAN [2] is the early work for learning multiple-domain face translation, it takes multiple attributes as input, and transfer one face image from one domain to other domains. During the training, StarGAN exploits a reconstruction and cycle consistency loss to preserve the content of the input face. After that, many works have been improving StarGAN, such as AttGAN [51], STGAN [6], SSCGAN [53] and HifaFace [55]. However, these models operate on low-resolution data; they cannot manipulate 3D factors, such as camera poses.

Interpreting Latent Space of StyleGAN for Face Editing An alternative line of works explores the disentanglement of StyleGAN’s latent space for face editing. These approaches can be roughly classified into two types based on whether they use semantic labels: unsupervised methods and attribute-conditional methods. The former learns to discover interpretable directions in latent space by leveraging techniques such as Principal Component Analysis (PCA) [9], closed-form factorization [58], learnable orthogonal matrices [10], [11], and regularization losses [59], [60]. GANSpace [9] shows that PCA in the latent space of StyleGAN can find important interpretable directions that can be used to control image generation. To compute the PCA of the style codes, GANSpace samples multiple random

vectors (i.e., z space) and computes the corresponding style codes (i.e., \mathcal{W} space). To avoid the extensive data sampling of GANSpace, SeFa [58] directly decomposes the model weights with a closed-form solution. Similarly, recent works [10], [11] propose to obtain a disentangled latent space by learning an orthogonal matrix for editing latent code.

As far as we know, the attribute conditions can be of different types, including global-level (e.g., label vectors) and local-level (e.g., semantic segmentation maps) modalities. The first type [3], [61], [62] usually utilizes off-the-shelf attribute classifier networks to obtain the attribute vectors of training images and then uses these vectors as input. For example, StyleFlow [3] proposes to utilize conditional normalizing flow (CNF) to model the mapping from conditional labels and latent codes (z space) to intermediate vectors (\mathcal{W} space). StyleFlow trains the flow model (CNF) with triplets consisting of vectors sampled from \mathcal{W} space, corresponding faces, and predicted face attributes. Though StyleFlow can produce facial pose transformation, it suffers from serious view inconsistency as it lacks an understanding of the underlying 3D world. The second type utilizes the coarse masks [63] or predicts face semantics [64] with k-means.

Additionally, some methods [65], [66], [67], [68] also explore the semantic disentanglement of the model, but they redesign the StyleGAN; thus, they need to retrain the generator. For example, TransEditor [66] presents a transformer-based module for dual space interactions where one latent code is used as the key and value and the other as the query. This dual-space interaction helps disentangle the style and the content representations. Some works focus on local facial controls by integrating face parsing into generation [67] or by adding spatial information for styles code with the conv-based module [68].

Overall, these StyleGAN-based models have demonstrated the ability to produce high-quality images and perform precise editing. However, they fail to change the facial pose and preserve view consistency due to a lack of 3D modeling abilities.

3DMM-Guided Face Generation and Editing. Recently, some works [4], [5], [12], [69], [70] demonstrate high-quality control over GAN generation via a 3DMM [13]. 3DMM is the 3D Morphable Face Model parameterized by the face shape, expression, and texture. For example, Geng *et al.* [69] utilizes 3DMM to guide fine-grained face manipulation for arbitrary expression transfer. First, they extract texture and shape coefficients by fitting 3DMM to each real face in the dataset. Then, they utilize the texture generator to create the target textures with the source texture and the target expression and utilize the shape predictor to produce the target shape with the source shape coefficients and the target expression as input. Finally, the global generator utilizes rendered faces and the target expression to produce the final faces. StyleRig [4] and DiscoFaceGAN [12] use 3DMM to manipulate the latent space of StyleGAN. While StyleRig is based on pre-trained StyleGAN models and only tunes a DFR module that learns the mapping from latent code to the coefficients of 3DMM. On the other hand, DiscoFaceGAN re-trains the entire model. It exploits multiple VAE to model the distribution of 3DMM coefficients and introduces self-

supervised losses to disentangle different factors. Compared to these models, our model does not require a 3DMM prior and still achieves better multi-view consistency. Additionally, our models can achieve more variable face editing, such as hair color and age.

Finally, Shi *et al.* [5] presents a LiftedGAN model, which lifts the pre-trained StyleGAN2 in 3D. This model is free of 3DMM prior. However, this model cannot achieve attribute-conditional control.

GAN Inversion for Real Face Editing. GAN inversion aims to find an optimal latent code corresponding to a given real image and has been widely used for real image editing tasks. The previous methods can be divided into two broad categories: optimization-based [71], [72], [73] and encoder-based [74], [75], [76], [77]. For example, Roich *et al.* [73] presents a novel optimization-based method called Pivotal Tuning Inversion (PTI). In PTI, they first obtain the optimized latent code as the pivot by fixing the parameters of the generator, then fix this pivot and finetune the generator parameters to obtain better reconstruction while preserving the editing abilities of the latent code. After the inversion step, they utilize the popular latent-disentanglement method, such as InterfaceGAN or GANSpace, for face editing. In this paper, we use the PTI for GAN inversion. Concurrent with our work, some methods [26], [78], [79], [80] employ 3D-aware GAN as a basic model instead of StyleGAN to achieve multi-view consistent face editing guided by the segmentation masks. They also apply GAN inversion to project real images into latent space for editing. Different from these methods with segmentation masks, we use attribute labels to guide face editing.

3 THE PROPOSED METHOD

We introduce the 3D-aware GAN with generative neural radiance fields (GNeRF). Our method can work with most of GNeRF backbones, and we showcase it with the two most recent ones, StyleSDF [22] and EG3D [23]. Since they have similar architecture, we only describe StyleSDF [22]. Then, we detail the ‘Training-As-Init, Optimizing-for-Tuning’ (TRIOT) method. In the training stage, we introduce the previous StyleFlow, using the continuous normalized flows to attain the initial latent code corresponding to the target labels. Then, we introduce the optimization stage with the attribute-specific consistency losses to search for better latent codes that preserve non-target regions and provide more accurate target-region editing. Finally, we introduce a new method for the reference-based geometry transfer.

3.1 Generative Neural Radiance Fields (GNeRF)

NeRF [14] is a continuous neural mapping M that maps a 3D position \mathbf{x} and a 2D viewing direction \mathbf{v} to the rgb color \mathbf{c} and density σ :

$$(\mathbf{c}, \sigma) = \mathcal{M}(\gamma(\mathbf{x}), \gamma(\mathbf{v})), \quad (1)$$

where γ indicates the positional encoding mapping function.

GNeRF, such as GRAF [38], is a conditional variant of NeRF. Unlike NeRF, which requires multiple views of a single scene with estimated camera poses, GNeRF can be

trained with unposed 2D images from different scenes. In Pi-GAN [20], GNeRF is trained with adversarial learning and conditioned on a latent code \mathbf{z} :

$$(\mathbf{c}, \sigma) = \mathcal{M}(\gamma(\mathbf{x}), \gamma(\mathbf{v}), \mathbf{z}), \quad (2)$$

where the latent code \mathbf{z} with following MLP layers aims to infer frequencies α and shifts β of a SIREN layer [20].

StyleSDF. As shown in Fig. 2, StyleSDF also adopts the SIREN layers inside GNeRF. However, it utilizes Signed Distance Fields (SDF) to improve the GNeRF and add a 2D StyleGAN generator as a second-stage rendering. In the first stage, the GNeRF is trained separately. It produces a feature vector \mathbf{f} , RGB color \mathbf{c} and SDF values \mathbf{d} :

$$(\mathbf{f}, \mathbf{c}, \mathbf{d}) = \mathcal{M}(\gamma(\mathbf{x}), \gamma(\mathbf{v}), \mathbf{w}), \quad (3)$$

where the learned SDF values define the object surface and thus allow the extract of the mesh via Marching Cubes [81]. Moreover, \mathbf{d} will be converted into the density σ for volume rendering.

The RGB color \mathbf{c} is later rendered into the low-resolution face image using the classical volume rendering. The output image is then used as input for the discriminator.

In the second stage, all GNeRF parameters are fixed. The feature vector \mathbf{f} is volume-rendered into low-resolution feature map \mathbf{F} , which is then mapped into a high-resolution result using Style-based convolutional modules. This high-resolution image is passed to another discriminator.

3.2 Training-as-Init, Optimizing-for-Tuning with Attribute-Specific Consistency Losses

The pre-trained StyleSDF (or EG3D) is our model’s backbone. Training triplets are sampled from the pretrained StyleSDF model: latent vector \mathbf{w} ($\mathcal{W}+$ space), the corresponding generated sample \mathbf{I} along with its low-resolution \mathbf{I}_L version and attribute labels \mathbf{A} predicted by the *off-the-shelf* attribute classifiers. As mentioned above, our proposed TRIOT has two stages. In the training stage, the pre-trained StyleSDF is then extended with the continuous normalized flows module, which is trained using the latent vectors and labels and then can manipulate the latent code to enable 3D-aware attribute editing in the inference time. More details will be introduced below.

Training Stage with Continuous Normalized Flows. We followed StyleFlow to use continuous normalized Flows (CNF) to learn the conditional distribution of latent code \mathbf{w} . Normalized Flows are a type of generative model to map the prior distribution $\mathbf{z} \sim p_{\mathbf{z}}$ to a more complex distribution $\mathbf{x} \sim p_{\mathbf{x}}$, where the basic blocks of a normalizing flow is an invertible transformation $\mathbf{x} = f(\mathbf{z})$. Let define $f = f_1 \circ f_2, \dots, \circ f_n$, we have $\mathbf{x}_n = f_n \circ \dots, f_2 \circ f_1(\mathbf{x}_0)$. Then, it can be shown that f is also bijective and invertible. Though a chain of mapping f_i , $p(\mathbf{x}_n)$ can be represented as using discrete normalized flows:

$$\ln p_n(\mathbf{x}_n) = \ln p_0(\mathbf{x}_0) - \sum_{i=1}^n \ln \left| \det \frac{df_i}{d\mathbf{x}_{i-1}} \right|. \quad (4)$$

where the function f_i can be modeled by a neural network.

StyleFlow uses the continuous normalized flows instead of the discrete normalized flows (DNF) to avoid the costly



Fig. 3. Corresponding mask M for all attributes.

computation of Jacobian determinants in DNF while ensuring learning a reversible mapping. Specifically, the change in log density is:

$$\ln p(\mathbf{x}_{t_i}) = \ln p(\mathbf{x}_{t_{i-1}}) - \int_{t_{i-1}}^{t_i} \text{Tr} \left(\frac{dF}{d\mathbf{x}_t} \right) dx, \quad (5)$$

where t is the time variable in CNF. We use some CNF blocks to represent the function F , then train the CNF blocks using the latent code \mathbf{w} and the corresponding condition \mathbf{A} . In the reference stage, we reversely inference the \mathbf{z}_r from \mathbf{w}_r using the original labels \mathbf{A}_r as the condition, then transfer \mathbf{w}_r to new latent code \mathbf{w}_e given target labels \mathbf{A}_e by the forward inference.

Optimization Stage with Attribute-Specific Consistency Losses. After training, we can edit latent code to generate view-consistent images with modified attributes. However, editing some attributes can affect unrelated attributes, especially the local ones. For example, converting a “No-Smile” face into a “Smile” can modify the identity. It is due to the entanglement of latent codes for some of the attributes. To alleviate this problem, we propose an optimization stage to search for better latent codes corresponding to the better trade-off between the preservation of non-target regions and target-region editing. As shown in the Fig. 3, we defined an attribute-specific mask \mathbf{M} for different attributes. For global attributes, i.e., “Gender”, and “Age”, we focus on preserving the background and clothes. Thus, we use an *off-the-shelf* face parsing model [82] to obtain the corresponding background and clothes region. For other local attributes, we pre-defined the rectangular mask for every attribute. Given this mask, we select the non-target region \mathbf{M} and target region $1 - \mathbf{M}$. As shown in the right of Fig. 2, we obtain: $\mathbf{I}_r, \mathbf{I}_r^n, \mathbf{I}_e, \mathbf{I}_e^n$, and an initial latent code \mathbf{w}_e . Given the corresponding optimization objection, we aim to find an optimal latent code $\hat{\mathbf{w}}_e$, corresponding image $\hat{\mathbf{I}}_e$ and normal map $\hat{\mathbf{I}}_e^n$.

Specifically, our objective functions are attribute-specific and consist of two parts: geometry consistency loss and texture consistency loss. As shown in the right of Fig. 2, our texture and geometry consistency optimization objection is defined as follows:

$$\begin{aligned} \hat{\mathbf{w}}_e &= \arg \min_{\hat{\mathbf{w}}_e} \|\mathbf{M} \odot (\hat{\mathbf{I}}_e - \mathbf{I}_r)\|_1 \\ &+ \|(1 - \mathbf{M}) \odot (\hat{\mathbf{I}}_e - \mathbf{I}_e)\|_1, \\ &+ \|\mathbf{M} \odot (\hat{\mathbf{I}}_e^n - \mathbf{I}_r^n)\|_1 \\ &+ \|(1 - \mathbf{M}) \odot (\hat{\mathbf{I}}_e^n - \mathbf{I}_e^n)\|_1. \end{aligned} \quad (6)$$

This texture loss (First two items of Eq. 6) reduces differences between the reconstructed texture \mathbf{I}_r and the optimized texture $\hat{\mathbf{I}}_e$ in the non-target region while keeping $\hat{\mathbf{I}}_e$ the same as \mathbf{I}_e in the target region for attribute-editing. The geometry consistency loss (The last two items of Eq. 6) has the same objective function as the texture loss.

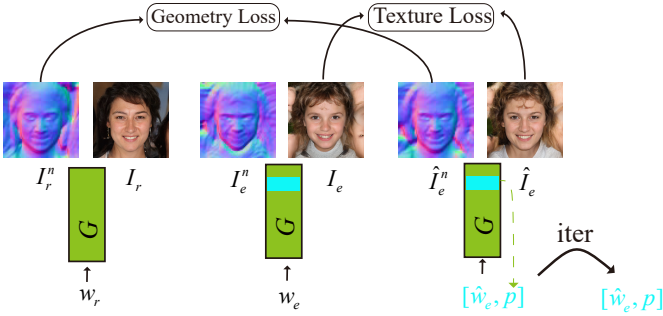


Fig. 4. Reference-based geometry transfer pipeline. It minimizes the difference between normals (geometry loss) and the differences between texture images (texture loss) in perceptual space to search for a better \hat{w}_e . Meanwhile, partial parameters p of generator G will be tuned.

By optimizing the latent code \hat{w}_e iteratively, we can achieve better editing results and preserve non-target regions in less than 1,000 iterations.

3.3 Reference-Based Geometry Transfer

Our model can achieve reference-based geometry manipulation by transferring the geometry from a reference face into a target face while preserving the target face’s appearance. Like TRIOT, the optimization objection includes two parts: the geometry consistency loss and the texture consistency loss. Given a reference image and corresponding normal map, we minimize the differences between reference and target normals (geometry loss) and the differences between the input image and target image (texture loss) in perceptual space. To fully utilize NeRF networks’ disentanglement of geometry and textures, we also optimize NeRF’s RGB-branches parameters p and the latent code w_e . We observe that tuning of partial networks can achieve a more accurate geometry transfer.

As shown in the Fig. 4, given the original latent code w_e and reference code w_r , the corresponding face image and normal pairs are (I_e, I_e^n) (I_r, I_r^n) , respectively. We use \hat{w}_e as the target code of the optimization pipeline with corresponding face image and normal pairs (\hat{I}_e, \hat{I}_e^n) . The optimization objective functions are defined as:

$$\hat{w}_e, p = \arg \min_{(\hat{w}_e, p)} LPIPS(I_e, \hat{I}_e) + \|(I_r^n - \hat{I}_e^n)\|_1. \quad (7)$$

This optimization stage can efficiently find a latent code for accurate reference-based geometry editing within hundreds of steps.

3.4 GAN Inversion

We utilize the state-of-the-art GAN Inversion method (PTI) to project real images into the latent space of our 3D-GAN. Then, we perform real image editing with our proposed TRIOT methods. In detail, we follow two steps of PTI: 1) optimizing the latent code to obtain the corresponding projected latent of the real image while fixing the generator parameters (including CNF Blocks); 2) fixing the optimized latent code and the parameters of CNF parameters while tuning the remaining parameters of the generator. Then, given the generator’s tuning parameters and projected latent code w as the initial point, we used the proposed TRIOT

method to search for better latent code following the texture and geometry consistency loss. Afterward, we can achieve accurate image editing for given real images.

4 EXPERIMENTS

We name our method TT-GNeRF (Training and Tuning Generative Neural Radiance Field) and use TT-GNeRF (S) and TT-GNeRF (E) to refer to our method with two different backbones: StyleSDF [22] and EG3D [23], respectively. We refer to the demo video¹ for more results about multiple-view attribute editing, reference-based geometry editing, and GAN inversion for real image editing.

4.1 Setting

Dataset. Given that the two backbones (*i.e.*, StyleSDF and EG3D) are trained on the FFHQ dataset [7], we train our model using sampled images and their corresponding latent codes. We use 40,000 images for training StyleSDF and 40,000 for EG3d. We employ *off-the-shelf* attribute-classifiers [8] to obtain six attribute labels, including Hair Color, Gender, Bangs, Age, Expression (Smiling), and Beard. We use all generated triplets to train our models.

Implementation Details. To speed up the training and reduce memory consumption, we compute the reconstruction and adversarial losses using the low-resolution images rendered from RGB values c . In the training stage, CNF Blocks are trained with the Adam optimizer [83] $\beta_1=0.9$, $\beta_2=0.999$, and a learning rate= $1e-4$ for 10,000 steps. In the optimization stage, we also use the Adam optimizer with $\beta_1=0.9$, $\beta_2=0.99$, and learning rate= $5e-4$. In this stage, the steps are set to 150 for global attributes and 300 for local attributes.

Compared Baselines. Since our method is an attribute-conditioned generative model, the most similar supervised method is StyleFlow [3], which can be used for face attribute editing tasks and multiple-view generation. To ensure a fair comparison, we extend the original Styleflow, which manipulates the latent space of a 2D generator, to work with 3D-Aware generators, *i.e.*, EG3D and StyleSDF. Moreover, we adopt the state-of-the-art generative model, TransEditor [66] as our baseline for comparing face semantic disentanglement with multiple-view generation results. We also compare with the 3DMM-guided model, DiscoFaceGAN [12]. Note that this model can only edit some expression-related attributes, such as “Smile”. We adopt a 3D-Aware LiftedGAN [5] to compare multiple-view generation. However, LiftedGAN cannot control individual attributes. LENErf [48] is a very similar model to our TT-GNeRF, but it does not release the code. DragGAN [84] also optimizes the latent space of GAN to achieve image editing. We do not compare our method with DragGAN as it focuses on the semantic control of 2D GAN. For real image editing, we compare our method with StyleFlow [3] and GOAE [85]. GOAE is the state-of-the-art 3D-aware image inversion and editing method.

Evaluation Metrics. Five metrics are used for evaluation: FID (Fréchet Inception Distance) score [86] to evaluate the

1. <https://ttgnerf.github.io/TT-GNeRF/>

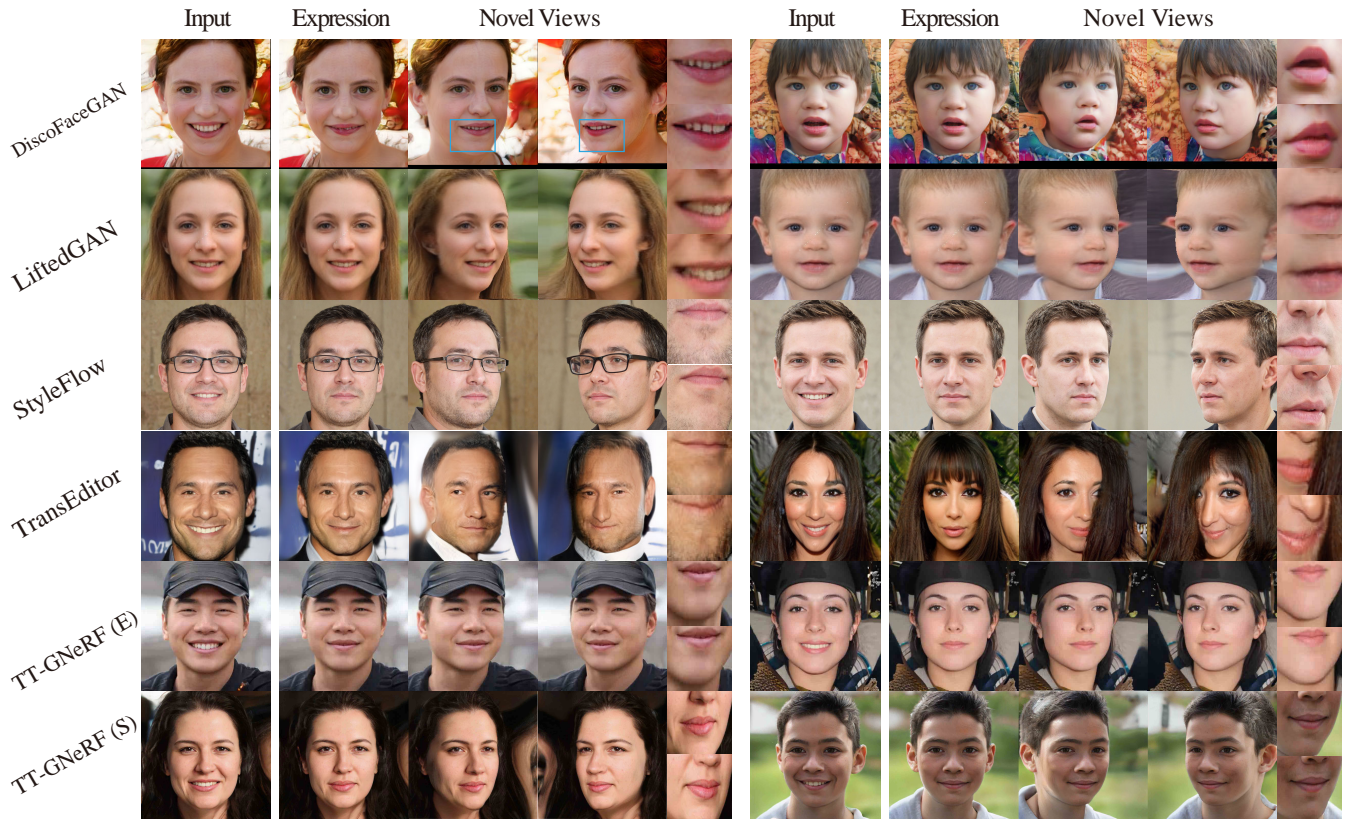


Fig. 5. Qualitative comparisons between our method and the baselines, *i.e.*, DiscoFaceGAN [12], LiftedGAN [5], StyleFlow [3], and TransEditor [66] on “Expression” attribute and the corresponding multiple-view renderings.

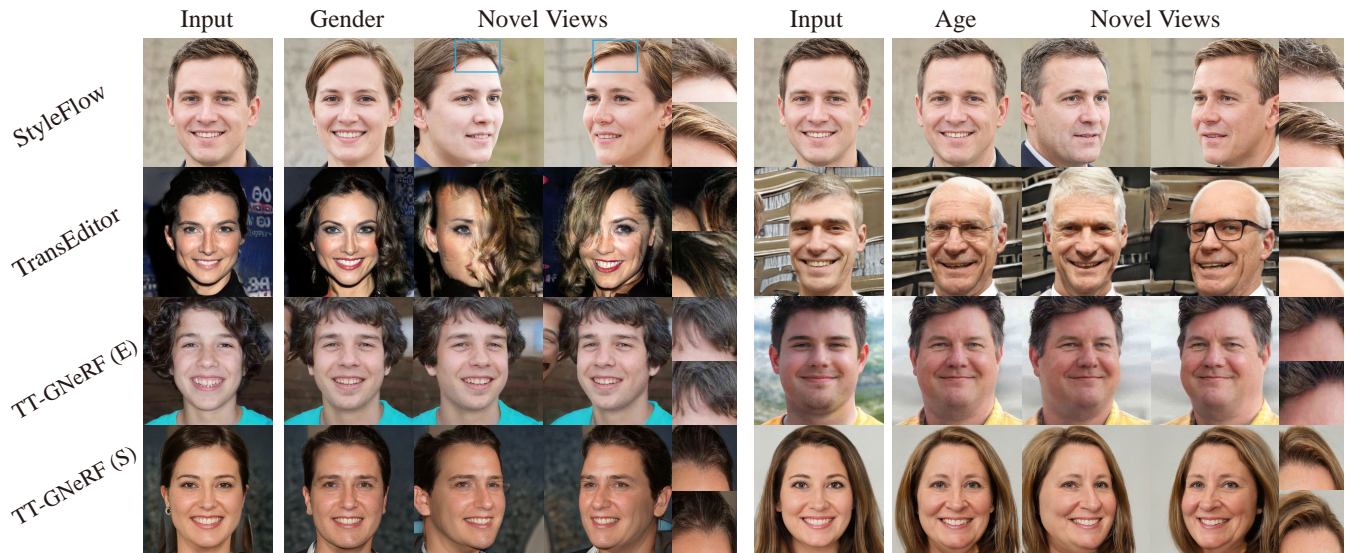


Fig. 6. Qualitative comparisons between our method and the baselines, *i.e.*, StyleFlow [3], and TransEditor [66] on “Gender” and “Age” attributes and the corresponding multiple-view renderings. Note that DiscoFaceGAN and LiftedGAN cannot deal with these two attributes.

quality and diversity of edited results; Classification Accuracy (CA) to evaluate the correctness of edited attributes; average Matching points (aMP) [87] and Face Recognition Similarity (FRS) [61] to quantitatively evaluate the consistency of multiple-view generation results; and Local Preservation (LP) to evaluate the preservation of non-target regions in editing results.

To evaluate the quality and diversity of the edited results, we calculate the FID score [86] by using samples

from FFHQ as the real distribution and the original image and its edited results as the fake distribution. To calculate FID scores, we sample 5000 real and fake samples from all models for each attribute. A lower FID score indicates a lower discrepancy between the image quality of the real and generated images.

To evaluate the accuracy of the attribute transfer, we use the *off-the-shelf* classifiers [8] to classify the edited samples and compute the accuracy by comparing the predicted and

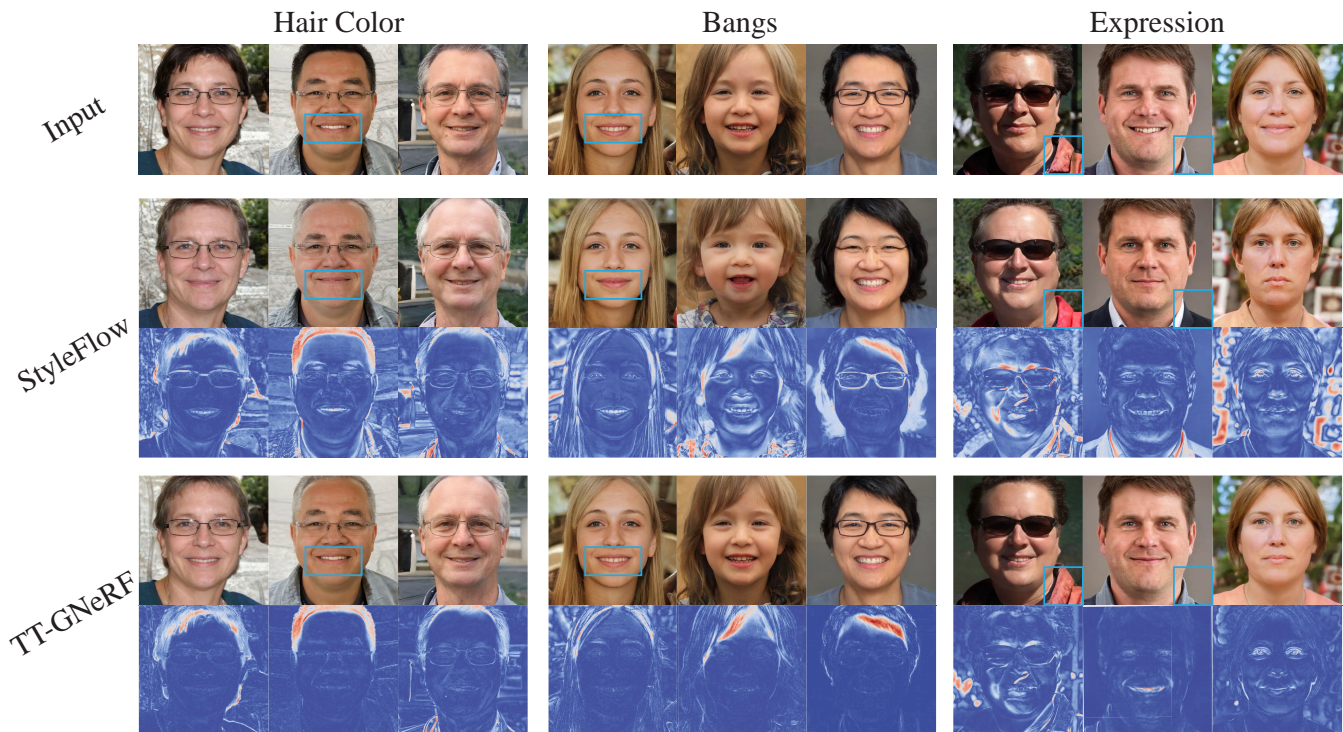


Fig. 7. Qualitative comparisons between our method and Styleflow based on EG3D.

TABLE 1

Quantitative results on the attributes editing results using four metrics: FID, Classification Accuracy (CA), Average Matching Point (aMP), and Face Recognition Similarity (FRS).

Method	Expression				Gender				Age			
	FID ↓	CA ↑	aMP ↑	FRS ↑	FID ↓	CA ↑	aMP ↑	FRS ↑	FID ↓	CA ↑	aMP ↑	FRS ↑
DiscoFaceGAN [12]	77.84	55.0	1347.4	0.587	-	-	-	-	-	-	-	-
LiftedGAN [5]	95.25	-	1484.0	0.464	-	-	-	-	-	-	-	-
StyleFlow [3]	78.98	99.2	1089.7	0.586	82.80	79.9	1088.4	0.588	95.61	89.9	1090.8	0.586
TransEditor [66]	55.97	90.5	1075.6	0.564	76.73	96.3	964.30	0.575	78.32	99.5	959.82	0.490
TT-GNeRF (E)	60.54	94.2	1538.5	0.858	58.20	98.0	1528.6	0.825	55.90	97.5	1632.7	0.878
TT-GNeRF (S)	58.55	95.4	1878.2	0.848	54.80	98.1	1825.1	0.822	55.43	90.4	1972.4	0.812

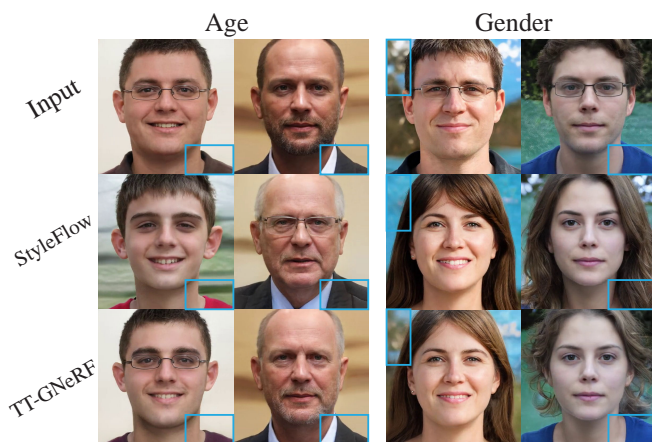


Fig. 8. Qualitative comparisons between our method and Styleflow based on EG3D.

the target labels. We refer to this metric as Classification Accuracy (CA). We calculate the CA using 1000 edited samples from all models for each attribute. Higher CA indicates better accuracy.

Evaluating view consistency without ground truth is a challenging task. We use proxy metrics such as the average Matched Points metric [87] to address this challenge. This metric involves computing a point-wise matching between two images (I_1, I_2) generated from the same identity but with different viewpoints using Patch2Pix [88] and counting the number of Matched Points $MP(I_1, I_2)$. We calculate the mean of MP across all pairs of samples for 100 random identities with ten views each to obtain a final *average MP* (aMP) score.

Additionally, we use Face Recognition Similarity (FRS) [61] to evaluate identity preservation across different views. Specifically, we use ArcFace [89], a state-of-the-art face recognition method, to estimate feature similarity between two facial images and compute the average score across 1000 samples with ten different views and 100 identities. Higher aMP and FRS scores indicate that synthesized images with different viewpoints have more similar identities to input faces.

We use 1000 input-edited paired samples to evaluate the Local Preservation score (LP) for local attributes, such as “Expression”. For every paired sample, we use the defined

TABLE 2

Quantitative evaluation of the editing and preservation trade-off between our method and StyleFlow, based on the StyleSDF. We use two metrics, CA and LP, to evaluate the editing of three attributes: Expression, Gender, and Age. Note that we define the non-target region by the mask of Fig. 3 to compute LP for three attributes.

Method	Expression		Gender		Age	
	CA \uparrow	LP \downarrow	CA \uparrow	LP \downarrow	CA \uparrow	LP \downarrow
StyleFlow [3]	97.1	29.62	100	17.99	95.3	19.60
TT-GNeRF (E)	94.2	17.48	98.0	9.104	97.5	8.002

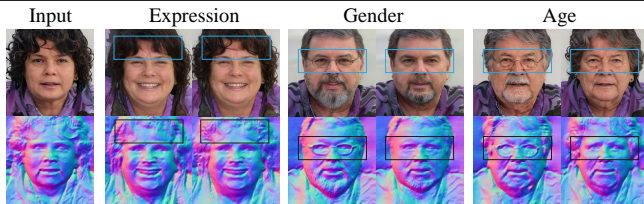


Fig. 9. Ablations for the geometry consistency loss. For each attribute, the first and second columns show the *w/o* or *w/* using the geometry consistency loss in the optimization stage, respectively.

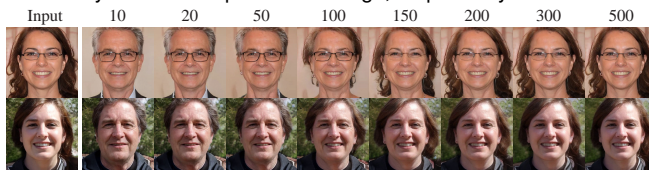


Fig. 10. Ablations for the optimization steps. The attribute “Age” editing results are shown in the 2nd-9th columns.

masks of Fig. 3 to attain the non-target region. Then, we measure the differences between each paired sample using ℓ_1 distance and average them across all pairs.

We found that LiftedGAN and DiscoFaceGAN cannot directly perform editing tasks for some attributes, such as “Gender” and “Age”. As a result, we do not provide scores for these methods. Instead, we provide the FID, aMP, and FRS scores for LiftedGAN using randomly generated samples rather than attribute-edited samples.

4.2 State-of-the-Art Comparison

We compare our method to baselines on facial attribute editing with multiple-view generation in Fig. 5 and Fig. 6. As aforementioned, we use “Expression”, “Gender” and “Age” attributes as examples since most baselines can directly edit these three attributes. Fig. 5 shows the results for “Expression” editing. We can observe that most models can accurately transfer from “Smile” to “No-Smile” while preserving non-target region well. However, TransEditor [66] fails to preserve the non-target region, as shown in the 4-th row of Fig. 5. Moreover, our method outperforms all baselines in the 3D consistency for novel-view generation of edited results. For example, DiscoFaceGAN cannot maintain hair color when changing pose, and expression changes compared to the original view when zooming in on the mouth. StyleFlow and TransEditor struggle with large pose variations and suffer from severe view-inconsistency problems, resulting in significant identity changes such as beard growth on zoomed-in mouths. LiftedGAN has improved 3D consistency but has limited quality and cannot perform facial attribute editing. Fig. 6 shows our method’s superiority

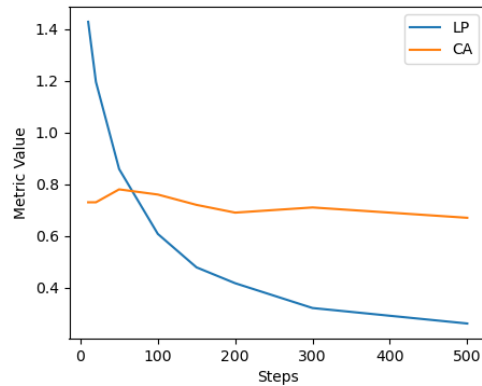


Fig. 11. Ablations for the optimization steps. The corresponding LP and CA scores are shown for different optimization steps. Note that we rescale the LP value.

in 3D consistency compared to other methods for “Gender” and “Age” editing results; please see the zoomed-in hair region for detailed comparisons.

Table 1 shows the quantitative evaluation results of “Expression”, “Gender”, and “Age” attributes editing. Our models achieve comparable performance to baselines for all three attributes regarding FID scores. Specifically, our TT-GNeRF (S) achieves the best FID scores for the “Gender” and “Age” attributes and a comparable score to TransEditor for the “Expression” attribute. Our models are also competitive with the baselines in terms of CA; for example, TT-GNeRF (S) achieves a score of 98.1 compared to 79.9 of StyleFlow and 96.3 of TransEditor for the “Gender” attribute. However, both models perform worse than the previous baselines for the “Expression” attribute. Table 1 shows that our models outperform previous methods on both aMP and FRS metrics for all three attributes; specifically, our TT-GNeRF (S) model achieves an aMP score of 1878.2 and an FRS score of 0.848 for the “Expression” attribute, better than LiftedGAN’s scores of 1484.0 aMP and 0.464 FRS and DiscoFaceGAN’s scores of 1347.4 aMP and 0.587 FRS.

Fig. 7 and Fig. 8 compare the attribute editing results between TT-GNeRF and StyleFlow using the same 3D-Aware generator. Fig. 7 shows the editing results for local attributes. We use the heatmap to visualize the input and editing results differences. For the attribute “Hair color”, the 2nd column shows that our TT-GNeRF can preserve the expression and skin color, but StyleFlow significantly changes both attributes. Similar results also can be found in the 1st column for “Bangs” results. For other results, we can observe that our model can better preserve the identity or the clothes than StyleFlow.

Fig. 8 shows the editing results for global attributes. We define the background and clothes as the non-target region for global attributes. For attribute “Age”, the clothes of our editing results are more similar to input than StyleFlow. For Attribute “Gender”, TT-GNeRF can preserve the background and clothes regions, which validates the effectiveness of our proposed consistency losses in the optimization stage.

Our TT-GNeRF achieves a better trade-off between editing and preservation than StyleFlow. This conclusion is

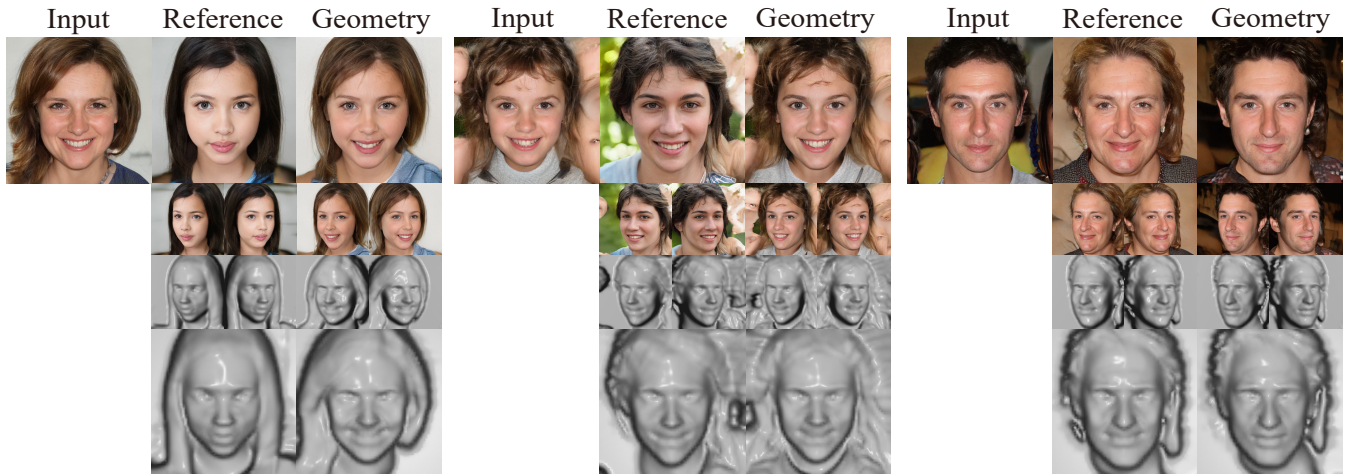


Fig. 12. Visual results of reference-based geometry transfer from TT-GNeRF (S).

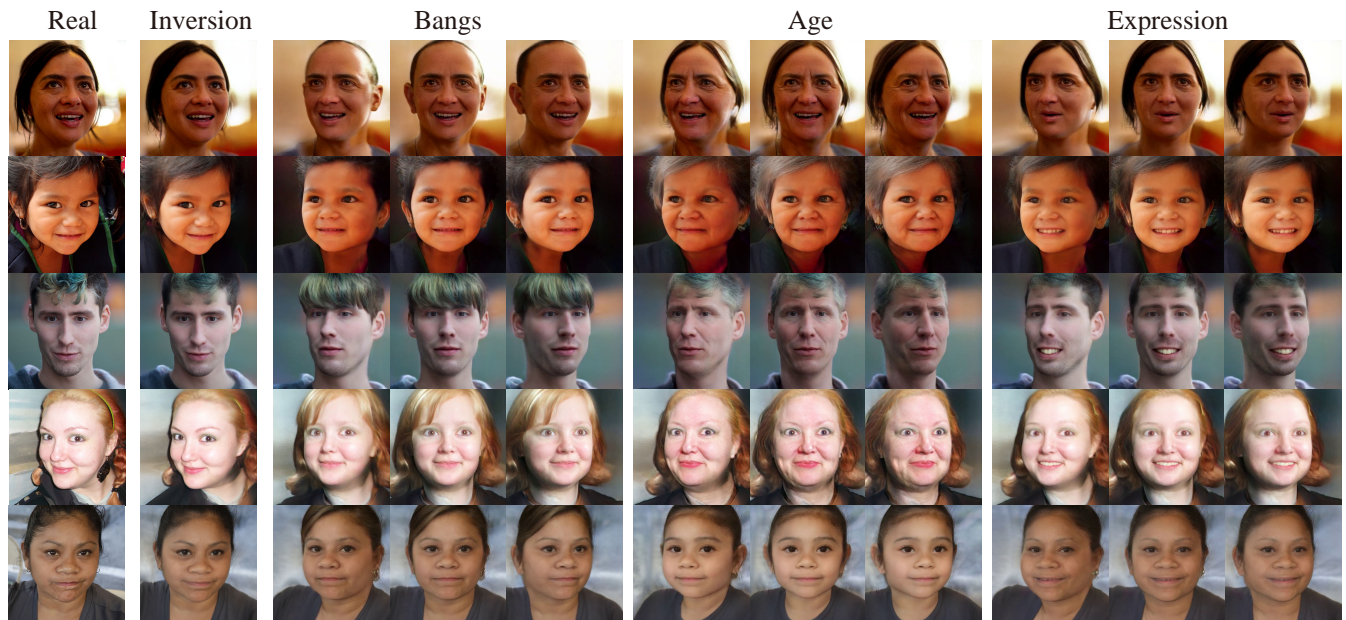


Fig. 13. GAN Inversion for real image editing and corresponding multiple-view generation. The results are obtained using TT-GNeRF (E) with the target attributes of “Bangs”, “Age” and “Smiling”.

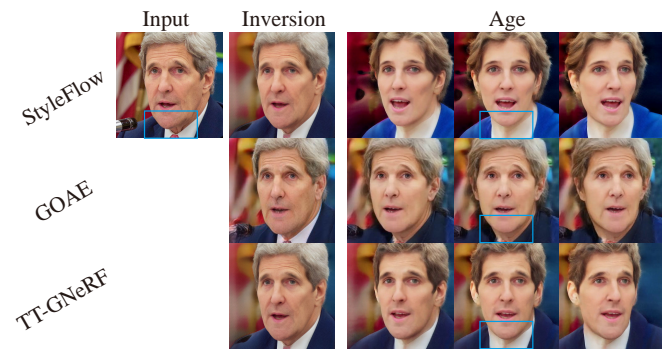


Fig. 14. The comparison of the editing results between StyleFlow [3], GOAE [85] and TT-GNeRF (Ours).

supported by the quantitative results in Table 2. In detail, TT-GNeRF attains a great improvement in LP score for all attributes while having a similar CA score to StyleFlow.

4.3 Ablation Study

In the following, we present ablation studies on the effect of the geometry consistency, and training steps in the optimization stage. As mentioned above, our training stage is based on StyleFlow. The ablation study for the optimization stage has been shown in Fig. 7, Fig. 8, and Table 2.

The geometry consistency Loss. Our proposed TRIOT can further improve identity preservation after face attribute editing. In the optimization stage, the objective function (Eq. 6) includes two parts: the texture consistency loss and the geometry consistency loss. We compare the full objective function with one ablation baseline, which removes the geometry losses. As shown in Fig. 9, we compare two methods by the attribute editing results. Specifically, for the attribute “Expression”, the full method can achieve better preservation in the background region, especially for the details (hair region within the rectangle box). For the other two attributes, we can observe that the *w/o* method cannot avoid the geometry changes, and the results have been

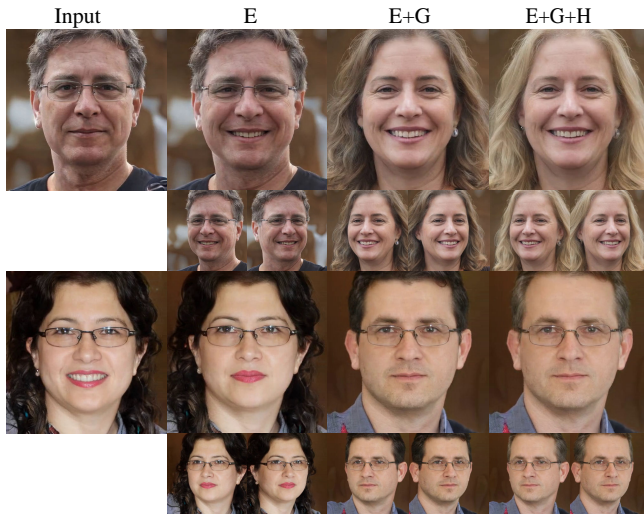


Fig. 15. Multiple-attribute editing results from our TT-GNeRF (E) method. E: Expression, G: Gender, H: Hair Color.

added with eyeglasses. The full method does not encounter a different problem.

The optimization steps. We study the effect of the steps of the optimization stage on the trade-off between the editing accuracy and the preservation of the identity (Or background). As shown in Fig. 10, we can observe that the aged results have different genders in the few steps setting. With more optimization steps, the aged results gradually get closer to the input. Fig. 11 also shows that the LP score becomes smaller as more steps are optimized, indicating that the input and results are closer. The CA also becomes smaller, indicating that attribute editing is also being weakened. Thus, we select the 100 or 150 steps setting which is the optimal trade-off between attribute editing and identity preservation.

4.4 Applications

Reference-based Geometry Transfer.

Disentangling geometry and textures is not easy to achieve in previous methods. We propose a simple optimization method for reference-based geometry transfer. Fig. 12 shows our geometry transferring results, corresponding multiple-view results and meshes. In the middle case, we can see that the face has been enlarged in size to match the geometry of the reference image while preserving appearance (e.g., identity and hair color).

GAN Inversion for Real Image Editing.

Fig. 13 shows real image inversion and editing results for “Bangs”, “Age” and “Expression” attributes. The 2-th column shows that we can produce almost perfect reconstruction for the real images. After that, our model can achieve accurate attribute editing. Fig. 14 shows the inversion and editing results from StyleFlow, GOAE, and ours. We observe that the non-target region is well preserved for our method, such as the clothes.

We refer to the demo video for more results about multiple-view attribute editing, reference-based geometry editing, and GAN inversion for real image editing.

Multiple-attribute Editing.

In addition to the previous single-attribute edits, our model can also perform sequential editing of multiple attributes. Fig. 15 shows high-quality edits for the sequence “Expression + Gender + Hair color”. Multiple-view results for these edits are presented at the bottom of each row, demonstrating that our model maintains strong 3D-view consistency in these cases.

5 CONCLUSIONS

In this work, we propose an attribute-conditional 3D-aware face generation and editing model, which shows the disentangling abilities of the generative neural radiance field with labels as inputs. Moreover, we integrate the training method for the normalized flows and the optimization method (TRIOT) into the 3D-aware face editing task to balance the best trade-off between quality and attribute-editing precision. Our model can achieve higher-quality 3D-aware face attribute editing compared to previous methods while better preserving the 3D consistency for different view generations. The qualitative and quantitative results demonstrate the superiority of our method. Additionally, our model can achieve reference-based geometry transfer tasks with the simple optimization method while preserving the appearance. However, there still exist some limitations. First, our model fails to edit the facial attribute in some cases. For example, the expression part of Table 1 shows that our CA score is worse than some methods. Second, our proposed TRIOT still costs some minutes for single attribute editing; thus, it is unacceptable for some real application scenarios. Finally, as shown in Fig. 13, our model can achieve the single image 3D model and perform attribute editing. However, compared to video-based head avatars [90], [91], the identity is not well preserved between real images and projected images. Proposing better GAN inversion techniques adapted for 3D-Aware GAN can further alleviate this problem.

REFERENCES

- [1] I. Goodfellow, J. Pouget-Abadie, M. Mirza, B. Xu, D. Warde-Farley, S. Ozair, A. Courville, and Y. Bengio, “Generative adversarial nets,” *Advances in neural information processing systems*, vol. 27, 2014.
- [2] Y. Choi, M. Choi, M. Kim, J.-W. Ha, S. Kim, and J. Choo, “Stargan: Unified generative adversarial networks for multi-domain image-to-image translation,” in *CVPR*, 2018.
- [3] R. Abdal, P. Zhu, N. J. Mitra, and P. Wonka, “Styleflow: Attribute-conditioned exploration of stylegan-generated images using conditional continuous normalizing flows,” *ACM Transactions on Graphics (TOG)*, vol. 40, no. 3, pp. 1–21, 2021.
- [4] A. Tewari, M. Elgharib, G. Bharaj, F. Bernard, H.-P. Seidel, P. Pérez, M. Zollhofer, and C. Theobalt, “Stylerig: Rigging stylegan for 3d control over portrait images,” in *Proceedings of the IEEE/CVF Conference on Computer Vision and Pattern Recognition*, 2020, pp. 6142–6151.
- [5] Y. Shi, D. Aggarwal, and A. K. Jain, “Lifting 2d stylegan for 3d-aware face generation,” in *Proceedings of the IEEE/CVF Conference on Computer Vision and Pattern Recognition*, 2021, pp. 6258–6266.
- [6] M. Liu, Y. Ding, M. Xia, X. Liu, E. Ding, W. Zuo, and S. Wen, “Stgan: A unified selective transfer network for arbitrary image attribute editing,” in *CVPR*, 2019, pp. 3673–3682.
- [7] T. Karras, S. Laine, and T. Aila, “A style-based generator architecture for generative adversarial networks,” in *Proceedings of the IEEE/CVF conference on computer vision and pattern recognition*, 2019, pp. 4401–4410.

- [8] T. Karras, S. Laine, M. Aittala, J. Hellsten, J. Lehtinen, and T. Aila, "Analyzing and improving the image quality of stylegan," in *Proceedings of the IEEE/CVF conference on computer vision and pattern recognition*, 2020, pp. 8110–8119.
- [9] E. Härkönen, A. Hertzmann, J. Lehtinen, and S. Paris, "Ganspace: Discovering interpretable gan controls," *Advances in Neural Information Processing Systems*, vol. 33, pp. 9841–9850, 2020.
- [10] Z. He, M. Kan, and S. Shan, "Eigengan: Layer-wise eigen-learning for gans," in *Proceedings of the IEEE/CVF International Conference on Computer Vision*, 2021, pp. 14408–14417.
- [11] A. Voynov and A. Babenko, "Unsupervised discovery of interpretable directions in the gan latent space," in *International conference on machine learning*. PMLR, 2020, pp. 9786–9796.
- [12] Y. Deng, J. Yang, D. Chen, F. Wen, and X. Tong, "Disentangled and controllable face image generation via 3d imitative-contrastive learning," in *Proceedings of the IEEE/CVF Conference on Computer Vision and Pattern Recognition*, 2020, pp. 5154–5163.
- [13] P. Paysan, R. Knothe, B. Amberg, S. Romdhani, and T. Vetter, "A 3d face model for pose and illumination invariant face recognition," in *2009 sixth IEEE international conference on advanced video and signal based surveillance*. Ieee, 2009, pp. 296–301.
- [14] B. Mildenhall, P. P. Srinivasan, M. Tancik, J. T. Barron, R. Ramamoorthi, and R. Ng, "Nerf: Representing scenes as neural radiance fields for view synthesis," in *ECCV*, 2020.
- [15] K. Zhang, G. Riegler, N. Snavely, and V. Koltun, "Nerf++: Analyzing and improving neural radiance fields," *arXiv preprint arXiv:2010.07492*, 2020.
- [16] T. Müller, A. Evans, C. Schied, and A. Keller, "Instant neural graphics primitives with a multiresolution hash encoding," *TOG*, Jan. 2022.
- [17] S. Peng, Y. Zhang, Y. Xu, Q. Wang, Q. Shuai, H. Bao, and X. Zhou, "Neural body: Implicit neural representations with structured latent codes for novel view synthesis of dynamic humans," in *CVPR*, 2021.
- [18] M. Tancik, V. Casser, X. Yan, S. Pradhan, B. Mildenhall, P. P. Srinivasan, J. T. Barron, and H. Kretschmar, "Block-nerf: Scalable large scene neural view synthesis," *arXiv preprint arXiv:2202.05263*, 2022.
- [19] L. Yen-Chen, P. Florence, J. T. Barron, A. Rodriguez, P. Isola, and T.-Y. Lin, "iNeRF: Inverting neural radiance fields for pose estimation," in *IEEE/RSSJ International Conference on Intelligent Robots and Systems (IROS)*, 2021.
- [20] E. Chan, M. Monteiro, P. Kellnhofer, J. Wu, and G. Wetzstein, "pi-gan: Periodic implicit generative adversarial networks for 3d-aware image synthesis," in *CVPR*, 2021.
- [21] M. Niemeyer and A. Geiger, "GIRAFFE: Representing scenes as compositional generative neural feature fields," in *CVPR*, 2021.
- [22] R. Or-El, X. Luo, M. Shan, E. Shechtman, J. J. Park, and I. Kemelmacher-Shlizerman, "StyleSDF: High-Resolution 3D-Consistent Image and Geometry Generation," *CVPR2022*, 2022.
- [23] E. R. Chan, C. Z. Lin, M. A. Chan, K. Nagano, B. Pan, S. De Mello, O. Gallo, L. Guibas, J. Tremblay, S. Khamis *et al.*, "Efficient geometry-aware 3d generative adversarial networks," *CVPR*, 2022.
- [24] X. Zhang, Z. Zheng, D. Gao, B. Zhang, P. Pan, and Y. Yang, "Multi-view consistent generative adversarial networks for 3d-aware image synthesis," *CVPR*, 2022.
- [25] Y. Xu, S. Peng, C. Yang, Y. Shen, and B. Zhou, "3d-aware image synthesis via learning structural and textural representations," *CVPR*, 2022.
- [26] J. Sun, X. Wang, Y. Zhang, X. Li, Q. Zhang, Y. Liu, and J. Wang, "Fenerf: Face editing in neural radiance fields," in *Proceedings of the IEEE/CVF Conference on Computer Vision and Pattern Recognition*, 2022, pp. 7672–7682.
- [27] K. Sun, S. Wu, Z. Huang, N. Zhang, Q. Wang, and H. Li, "Controllable 3d face synthesis with conditional generative occupancy fields," *NeurIPS*, 2022.
- [28] J. Sun, X. Wang, L. Wang, X. Li, Y. Zhang, H. Zhang, and Y. Liu, "Next3d: Generative neural texture rasterization for 3d-aware head avatars," *CVPR*, 2023.
- [29] C. Reiser, S. Peng, Y. Liao, and A. Geiger, "Kilonerf: Speeding up neural radiance fields with thousands of tiny mlps," in *ICCV*, 2021.
- [30] J. T. Barron, B. Mildenhall, M. Tancik, P. Hedman, R. Martin-Brualla, and P. P. Srinivasan, "Mip-nerf: A multiscale representation for anti-aliasing neural radiance fields," in *Proceedings of the IEEE/CVF International Conference on Computer Vision*, 2021, pp. 5855–5864.
- [31] M. Niemeyer, J. T. Barron, B. Mildenhall, M. S. M. Sajjadi, A. Geiger, and N. Radwan, "Regnerf: Regularizing neural radiance fields for view synthesis from sparse inputs," in *Proc. IEEE Conf. on Computer Vision and Pattern Recognition (CVPR)*, 2022.
- [32] J. T. Barron, B. Mildenhall, D. Verbin, P. P. Srinivasan, and P. Hedman, "Mip-nerf 360: Unbounded anti-aliased neural radiance fields," *CVPR*, 2022.
- [33] D. Verbin, P. Hedman, B. Mildenhall, T. Zickler, J. T. Barron, and P. P. Srinivasan, "Ref-NeRF: Structured view-dependent appearance for neural radiance fields," *CVPR*, 2022.
- [34] S. Peng, J. Dong, Q. Wang, S. Zhang, Q. Shuai, H. Bao, and X. Zhou, "Animatable neural radiance fields for human body modeling," in *ICCV*, 2021.
- [35] J. Gu, L. Liu, P. Wang, and C. Theobalt, "Stylenerf: A style-based 3d-aware generator for high-resolution image synthesis," *ICLR* 2022, 2022.
- [36] L. Ma, X. Li, J. Liao, X. Wang, Q. Zhang, J. Wang, and P. Sander, "Neural parameterization for dynamic human head editing," *TOG*, 2022.
- [37] R. Abdal, H.-Y. Lee, P. Zhu, M. Chai, A. Siarohin, P. Wonka, and S. Tulyakov, "3davatargan: Bridging domains for personalized editable avatars," *CVPR*, 2023.
- [38] K. Schwarz, Y. Liao, M. Niemeyer, and A. Geiger, "Graf: Generative radiance fields for 3d-aware image synthesis," in *NeurIPS*, 2020.
- [39] P. Henzler, N. J. Mitra, and T. Ritschel, "Escaping plato's cave: 3d shape from adversarial rendering," in *Proceedings of the IEEE/CVF International Conference on Computer Vision*, 2019, pp. 9984–9993.
- [40] T. Nguyen-Phuoc, C. Li, L. Theis, C. Richardt, and Y.-L. Yang, "Hologan: Unsupervised learning of 3d representations from natural images," in *Proceedings of the IEEE/CVF International Conference on Computer Vision*, 2019, pp. 7588–7597.
- [41] P. Zhou, L. Xie, B. Ni, and Q. Tian, "CIPS-3D: A 3D-Aware Generator of GANs Based on Conditionally-Independent Pixel Synthesis," 2021.
- [42] Y. Deng, J. Yang, J. Xiang, and X. Tong, "Gram: Generative radiance manifolds for 3d-aware image generation," 2022.
- [43] X. Pan, X. Xu, C. C. Loy, C. Theobalt, and B. Dai, "A shading-guided generative implicit model for shape-accurate 3d-aware image synthesis," *NeurIPS*, 2021.
- [44] Y. Xue, Y. Li, K. K. Singh, and Y. J. Lee, "Giraffe hd: A high-resolution 3d-aware generative model," *CVPR*, 2022.
- [45] K. Schwarz, A. Sauer, M. Niemeyer, Y. Liao, and A. Geiger, "Voxgraf: Fast 3d-aware image synthesis with sparse voxel grids," *NeurIPS*, 2022.
- [46] I. Skorokhodov, S. Tulyakov, Y. Wang, and P. Wonka, "Epigraf: Rethinking training of 3d gans," *arXiv preprint arXiv:2206.10535*, 2022.
- [47] J. Xiang, J. Yang, Y. Deng, and X. Tong, "Gram-hd: 3d-consistent image generation at high resolution with generative radiance manifolds," *arXiv preprint arXiv:2206.07255*, 2022.
- [48] J. Hyung, S. Hwang, D. Kim, H. Lee, and J. Choo, "Local 3d editing via 3d distillation of clip knowledge," in *Proceedings of the IEEE/CVF Conference on Computer Vision and Pattern Recognition*, 2023, pp. 12674–12684.
- [49] P. Isola, J.-Y. Zhu, T. Zhou, and A. A. Efros, "Image-to-image translation with conditional adversarial networks," *CVPR*, 2017.
- [50] J.-Y. Zhu, T. Park, P. Isola, and A. A. Efros, "Unpaired image-to-image translation using cycle-consistent adversarial networks," in *ICCV*, 2017.
- [51] Z. He, W. Zuo, M. Kan, S. Shan, and X. Chen, "Attgan: Facial attribute editing by only changing what you want," *IEEE Transactions on Image Processing*, vol. 28, no. 11, pp. 5464–5478, 2019.
- [52] P.-W. Wu, Y.-J. Lin, C.-H. Chang, E. Y. Chang, and S.-W. Liao, "Relgan: Multi-domain image-to-image translation via relative attributes," in *CVPR*, 2019.
- [53] W. Chu, Y. Tai, C. Wang, J. Li, F. Huang, and R. Ji, "Sscgan: Facial attribute editing via style skip connections," 2020.
- [54] Z. He, M. Kan, J. Zhang, and S. Shan, "Pa-gan: Progressive attention generative adversarial network for facial attribute editing," *arXiv preprint arXiv:2007.05892*, 2020.
- [55] Y. Gao, F. Wei, J. Bao, S. Gu, D. Chen, F. Wen, and Z. Lian, "High-fidelity and arbitrary face editing," in *CVPR*, 2021.
- [56] X. Chen, B. Ni, N. Liu, Z. Liu, Y. Jiang, L. Truong, and Q. Tian, "Coogan: A memory-efficient framework for high-resolution facial attribute editing," in *European Conference on Computer Vision*. Springer, 2020, pp. 670–686.

- [57] Y. Liu, E. Sangineto, Y. Chen, L. Bao, H. Zhang, N. Sebe, B. Lepri, W. Wang, and M. De Nadai, "Smoothing the disentangled latent style space for unsupervised image-to-image translation," in *Proceedings of the IEEE/CVF Conference on Computer Vision and Pattern Recognition (CVPR)*, 2021.
- [58] Y. Shen and B. Zhou, "Closed-form factorization of latent semantics in gans," in *CVPR*, 2021, pp. 1532–1540.
- [59] W. Peebles, J. Peebles, J.-Y. Zhu, A. Efros, and A. Torralba, "The hessian penalty: A weak prior for unsupervised disentanglement," in *European Conference on Computer Vision*. Springer, 2020, pp. 581–597.
- [60] Y. Wei, Y. Shi, X. Liu, Z. Ji, Y. Gao, Z. Wu, and W. Zuo, "Orthogonal jacobian regularization for unsupervised disentanglement in image generation," in *Proceedings of the IEEE/CVF International Conference on Computer Vision*, 2021, pp. 6721–6730.
- [61] Y. Liu, Y. Chen, L. Bao, N. Sebe, B. Lepri, and M. De Nadai, "Isf-gan: An implicit style function for high-resolution image-to-image translation," *TMM*, 2021.
- [62] H. Liang, X. Hou, and L. Shen, "Ssflow: Style-guided neural spline flows for face image manipulation," in *ACMMM*, 2021.
- [63] J. Zhu, Y. Shen, Y. Xu, D. Zhao, and Q. Chen, "Region-based semantic factorization in gans," *CVPR*, 2022.
- [64] E. Collins, R. Bala, B. Price, and S. Susstrunk, "Editing in style: Uncovering the local semantics of gans," in *Proceedings of the IEEE/CVF Conference on Computer Vision and Pattern Recognition*, 2020, pp. 5771–5780.
- [65] G. Kwon and J. C. Ye, "Diagonal attention and style-based gan for content-style disentanglement in image generation and translation," in *Proceedings of the IEEE/CVF International Conference on Computer Vision*, 2021, pp. 13980–13989.
- [66] Y. Xu, Y. Yin, L. Jiang, Q. Wu, C. Zheng, C. C. Loy, B. Dai, and W. Wu, "Transeditor: Transformer-based dual-space gan for highly controllable facial editing," *CVPR*, 2022.
- [67] Y. Shi, X. Yang, Y. Wan, and X. Shen, "Semanticstylegan: Learning compositional generative priors for controllable image synthesis and editing," *CVPR*, 2022.
- [68] H. Kim, Y. Choi, J. Kim, S. Yoo, and Y. Uh, "Exploiting spatial dimensions of latent in gan for real-time image editing," in *Proceedings of the IEEE/CVF Conference on Computer Vision and Pattern Recognition*, 2021, pp. 852–861.
- [69] Z. Geng, C. Cao, and S. Tulyakov, "3d guided fine-grained face manipulation," in *Proceedings of the IEEE/CVF Conference on Computer Vision and Pattern Recognition*, 2019, pp. 9821–9830.
- [70] C. Z. Lin, D. B. Lindell, E. R. Chan, and G. Wetzstein, "3d gan inversion for controllable portrait image animation," *arXiv preprint arXiv:2203.13441*, 2022.
- [71] R. Abdal, Y. Qin, and P. Wonka, "Image2stylegan: How to embed images into the stylegan latent space?" in *Proceedings of the IEEE/CVF International Conference on Computer Vision*, 2019, pp. 4432–4441.
- [72] —, "Image2stylegan++: How to edit the embedded images?" in *Proceedings of the IEEE/CVF Conference on Computer Vision and Pattern Recognition*, 2020, pp. 8296–8305.
- [73] D. Roich, R. Mokady, A. H. Bermano, and D. Cohen-Or, "Pivotal tuning for latent-based editing of real images," *arXiv preprint arXiv:2106.05744*, 2021.
- [74] J. Zhu, Y. Shen, D. Zhao, and B. Zhou, "In-domain gan inversion for real image editing," in *European conference on computer vision*. Springer, 2020, pp. 592–608.
- [75] E. Richardson, Y. Alaluf, O. Patashnik, Y. Nitzan, Y. Azar, S. Shapiro, and D. Cohen-Or, "Encoding in style: a stylegan encoder for image-to-image translation," in *Proceedings of the IEEE/CVF Conference on Computer Vision and Pattern Recognition*, 2021, pp. 2287–2296.
- [76] O. Tov, Y. Alaluf, Y. Nitzan, O. Patashnik, and D. Cohen-Or, "Designing an encoder for stylegan image manipulation," *ACM Transactions on Graphics (TOG)*, vol. 40, no. 4, pp. 1–14, 2021.
- [77] Y. Alaluf, O. Patashnik, and D. Cohen-Or, "Restyle: A residual-based stylegan encoder via iterative refinement," in *Proceedings of the IEEE/CVF International Conference on Computer Vision*, 2021, pp. 6711–6720.
- [78] J. Sun, X. Wang, Y. Shi, L. Wang, J. Wang, and Y. Liu, "Ide-3d: Interactive disentangled editing for high-resolution 3d-aware portrait synthesis," *TOG*, 2022.
- [79] Y. Chen, Q. Wu, C. Zheng, T.-J. Cham, and J. Cai, "Sem2nerf: Converting single-view semantic masks to neural radiance fields," *ECCV*, 2022.
- [80] K. Jiang, S.-Y. Chen, F.-L. Liu, H. Fu, and L. Gao, "Nerffaceediting: Disentangled face editing in neural radiance fields," in *SIGGRAPH Asia 2022 Conference Papers*, 2022, pp. 1–9.
- [81] W. E. Lorensen and H. E. Cline, "Marching cubes: A high resolution 3d surface construction algorithm," *ACM siggraph computer graphics*, vol. 21, no. 4, pp. 163–169, 1987.
- [82] C. Yu, J. Wang, C. Peng, C. Gao, G. Yu, and N. Sang, "Bisenet: Bilateral segmentation network for real-time semantic segmentation," in *Proceedings of the European conference on computer vision (ECCV)*, 2018, pp. 325–341.
- [83] D. P. Kingma and J. Ba, "Adam: A method for stochastic optimization," *ICLR*, 2014.
- [84] X. Pan, A. Tewari, T. Leimkühler, L. Liu, A. Meka, and C. Theobalt, "Drag your gan: Interactive point-based manipulation on the generative image manifold," in *ACM SIGGRAPH 2023 Conference Proceedings*, 2023.
- [85] Z. Yuan, Y. Zhu, Y. Li, H. Liu, and C. Yuan, "Make encoder great again in 3d gan inversion through geometry and occlusion-aware encoding," *ICCV*, 2023.
- [86] M. Heusel, H. Ramsauer, T. Unterthiner, B. Nessler, and S. Hochreiter, "Gans trained by a two time-scale update rule converge to a local nash equilibrium," in *NeurIPS*, 2017.
- [87] J. Zhang, E. Sangineto, H. Tang, A. Siarohin, Z. Zhong, N. Sebe, and W. Wang, "3d-aware semantic-guided generative model for human synthesis," *arXiv preprint arXiv:2112.01422*, 2021.
- [88] Q. Zhou, T. Sattler, and L. Leal-Taixe, "Patch2pix: Epipolar-guided pixel-level correspondences," in *CVPR*, 2021.
- [89] J. Deng, J. Guo, N. Xue, and S. Zafeiriou, "Arcface: Additive angular margin loss for deep face recognition," in *Proceedings of the IEEE/CVF conference on computer vision and pattern recognition*, 2019, pp. 4690–4699.
- [90] G. Gafni, J. Thies, M. Zollhofer, and M. Nießner, "Dynamic neural radiance fields for monocular 4d facial avatar reconstruction," in *Proceedings of the IEEE/CVF Conference on Computer Vision and Pattern Recognition*, 2021, pp. 8649–8658.
- [91] Y. Zheng, V. F. Abrevaya, M. C. Bühler, X. Chen, M. J. Black, and O. Hilliges, "Im avatar: Implicit morphable head avatars from videos," in *Proceedings of the IEEE/CVF Conference on Computer Vision and Pattern Recognition*, 2022, pp. 13545–13555.